

Wurtzite-to-tetragonal structure phase transformation and size effect in ZnO nanorods

J. Wang,^{1,2} P. Xiao,² M. Zhou,³ Z. R. Wang,⁴ and F. J. Ke^{1,2,a)}

¹*School of Physics and Nuclear Energy Engineering, Beihang University, Beijing 100191, People's Republic of China*

²*LNM, Institute of Mechanics, Chinese Academy of Sciences, Beijing 100190, People's Republic of China*

³*G.W.W. School of Mechanical Engineering, Georgia Institute of Technology, Atlanta, Georgia 30332-0405, USA and Department of Mechanical and Aerospace Engineering, Seoul National University, Seoul 151-742, Republic of Korea*

⁴*College of Sciences, Yanshan University, Qinhuangdao 066004, People's Republic of China*

(Received 13 August 2009; accepted 30 November 2009; published online 25 January 2010)

The deformation of [0001]-oriented ZnO nanorods with hexagonal cross sections under uniaxial tensile loading is analyzed through molecular statistical thermodynamics (MST) simulations. The focus is on the size dependence of mechanical behavior in ZnO nanorods with diameters ranging from 1.95 to 17.5 nm. An irreversible phase transformation from the wurtzite (P6₃mc space group) structure to a tetragonal structure (P4₂/mnm space group) occurs during the tensile loading process. Young's modulus before the transformation demonstrates a size dependence consistent with what is observed in experiments. A stronger size dependence of response is seen after the transformation and is attributed to the polycrystalline nature of the transformed structure. A comparison of the MST and molecular dynamics (MD) methods shows that MST is 60 times faster than MD and yields results consistent with the results of MD. © 2010 American Institute of Physics.

[doi:10.1063/1.3277053]

I. INTRODUCTION

Microstructure and phase transformation significantly affect the mechanical, thermal, phonic, electric, and magnetic properties of materials. Phase transformations can lead to significant changes in material behavior, giving rise to mechanisms for property enhancement and design of new devices. So far, six structures of ZnO have been reported, including wurtzite (WZ) (P6₃mc space group),¹ zincblende (ZB),² rocksalt (RS),³ a layered structure (LY),⁴ a hexagonal structure (HX) (Ref. 5), and a tetragonal structure (originally referred to as a body-centered-tetragonal structure with four-atom rings or BCT-4).^{6–8} WZ is the most stable and commonly observed phase at ambient conditions. ZB can be obtained only on cubic surfaces of certain crystals under specific growth conditions. The other four structures can be obtained via phase transformations from WZ under different loading conditions.^{5–7} Since WZ is the only structure showing piezoelectricity and has been used to fabricate nanogenerators,⁹ understanding the mechanisms and conditions of the transformations leading to the other structures is essential in the design of devices as the loss of piezoelectricity due to phase transformations can render devices inoperable.

A number of numerical techniques is available for calculating the physical properties of nanomaterials and each has its own advantages and disadvantages. *Ab initio* calculations based on, for example, the density functional theory (DFT) require no empirical input but are impractical for size scales of real devices. MD simulations can deal with size

scales larger than those for DFT and are now routinely used in many applications, but they are associated with very short time scales. Furthermore, consideration of macroscopic equilibrium (or quasistatic) conditions within the MD framework can be computationally intensive. While molecular statics considers equilibrium, it is only applicable at 0 K. Along this line, various frameworks have been developed recently. For instance, the quasicontinuum method¹⁰ imbues atomistic characteristics to finite element (FE) based continuum analyses. It is much less computationally intensive compared to MD and can deal with larger size scales, but it does not explicitly account for the discrete atomistic structure of materials. This method has recently been extended to finite temperatures.¹¹ Approaches^{12–15} that couple FE regions and MD regions can deal with size scales up to microns, but mismatches between the FE and MD regions lead to issues such as ghost forces and reflections. The molecular statistical thermodynamics (MST) method recently developed based on statistical thermodynamics and quantum mechanics^{16–18} is a method for analyzing macroscopic equilibrium (macroscopic “quasistatic”) processes at finite temperatures. It is an atomistic framework which allows explicit account for molecular structures of materials and can significantly reduce computational time compared to MD. Similarities and differences between MD and MST are listed in Table I.

Our previous MD simulations^{7,8} have shown that a metastable tetragonal phase can exist in [0001]-oriented ZnO nanorods under uniaxial tensile loading. Due to the computational time-intensive nature of MD for approximating macroscopic equilibrium conditions, only sizes up to 4.55 nm have been analyzed. Here, we combine both MD and MST simulations to analyze the deformation at 300 K of

^{a)}Author to whom correspondence should be addressed. Tel.: 86-10-82543939. FAX: 86-10-82543977. Electronic mail: kefj@lnm.imech.ac.cn.

TABLE I. Similarities and differences between MD and MST.

	MD	MST
Similarities		Atomistic or molecular potential Atomic or molecule mass
Differences		Minimization of Helmholtz free energy Boltzmann constant (k) Average atomic positions ($\bar{\mathbf{r}}_i$) Planck constant (h)
(1) Governing equation	Newton's equation of motion	
(2) Independent variables	Time step (t) Atomic positions (\mathbf{r}_i)	
(3) Algorithm	Finite difference solution of Newton's equation of motion	Numerical minimization of Helmholtz free energy

such rods with lateral dimensions between 1.95 and 17.5 nm. The benefit is the two methods can mutually reinforce each other and allow a large size range to be analyzed. Since the largest size (17.5 nm) in our simulation corresponds to the smallest size of ZnO nanorods tested in experiments,¹⁹ these computed results provide a reference for analyzing the size dependence of Young's modulus. Additionally, the MST methods also allow the minimal energy states associated with the phase transformation to be explicitly evaluated.

II. COMPUTATIONAL FRAMEWORK

The ZnO nanorods analyzed have hexagonal cross sections and the single crystalline WZ structure. The rod axis coincides with the [0001] crystalline direction and six {01 $\bar{1}$ 0} crystalline planes constitute the lateral surfaces, as illustrated in Fig. 1. Five different lateral sizes (1.95, 3.25, 4.55, 9.75, and 17.5 nm) are considered, all with the same length of 14.6 nm. The lattice constants for the WZ structure are $a = 3.25$ Å, $c = 5.21$ Å, and $u = 0.386$.¹ Here, $u = u_c/c$ denotes the relative offset between Zn and O basal planes along the [0001] orientation. The nanorods are generated by repeating a WZ unit cell along the [0001], [01 $\bar{1}$ 0], and [2 $\bar{1}$ 10] orientations. The supercell concept is used. Specifically, periodic boundary conditions are applied in the [0001] direction to approximate an infinitely long rod, and a vacuum of 3.0 nm is imposed outside the lateral surfaces to keep them traction-free. The temperature is maintained at 300 K. For direct comparison, numerical and geometrical conditions for the MST analysis here are taken to be the same as those in our previous MD simulations,⁷ except that the MST calculations also concern the two additional sizes of 9.75 and 17.5 nm, in addition to the sizes of 1.95, 3.25, and 4.55 nm analyzed before.

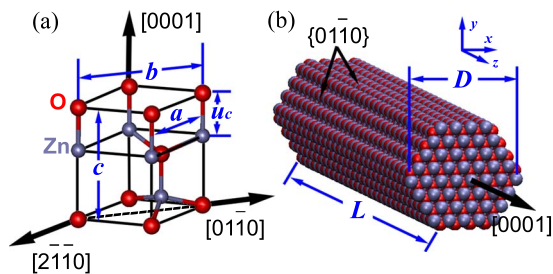


FIG. 1. (Color online) (a) Unit WZ cell, (b) ZnO nanorod with lateral dimension (d) of 1.95 nm and length (l) of 14.6 nm.

A. The MST method

In statistical physics, a solid at finite temperature can be regarded as an ensemble of atomic oscillators whose Helmholtz free energy can be expressed as a function of the oscillation frequencies. The core of MST is the particle-oscillator duality.^{17,18} In the analyses of mechanical deformation, the macroscopic statistical equilibrium positions of the atoms are used. On the other hand, when the Helmholtz free energy of the system is calculated, the thermal oscillations of the atoms are in focus. From the macroscopic perspective, statistically equilibrium (quasistatic) deformation is associated with the equilibrium configuration of the system which can be obtained by minimizing the Helmholtz free energy with respect to the statistical equilibrium positions of the atoms under the constraint of applied loading. The link between the oscillatory frequencies and the equilibrium positions of atoms can be deduced via the dynamical matrix \mathbf{D} of the atoms.²⁰ Specifically, for a system with N atoms at volume V and temperature T , the Helmholtz free energy F can be written as^{18,21,22}

$$F = \Phi + kT \sum_{j=1}^N \sum_{\alpha=1}^3 \ln \left[2 \sinh \left(\frac{\hbar \omega_{j\alpha}}{2kT} \right) \right]. \quad (1)$$

Here, Φ is the total interatomic potential, k is the Boltzmann constant, ω_j is the frequency of atom j , α is the α th coordinate, and \hbar is the reduced Planck constant. The second term on the right hand side in Eq. (1) accounts for the contribution of temperature and thermal motions of the atoms to the free energy. For Φ , a Buckingham-type pair potential for ZnO in the form of

$$\Phi = \sum_{i \neq j} \left[\frac{q_i q_j}{r_{ij}} + A \exp \left(\frac{-r_{ij}}{\rho} \right) - \frac{C}{r_{ij}^6} \right] \quad (2)$$

is used. This is the same potential as that used in our MD simulations.^{7,8} In the above relation, r_{ij} is the distance between ions i and j , q_i is the charge on ion i and A , and ρ and C are parameters^{23,24} whose values are listed in Table II. The first term of this potential represents long-range Coulomb electrostatic interactions and the last two terms represent short-range covalent interactions. It has been shown that this potential accurately captures the equilibrium energy, elastic constants, surface properties, and lattice constants for all existing polymorphs of ZnO.^{6,8,24,25} This is important for the

TABLE II. Short-range potential parameters for ZnO (Ref. 23).

Species	A (eV)	ρ (Å)	C (eV Å ⁶)
O ²⁻ -O ²⁻	9547.96	0.21916	32.0
Zn ²⁺ -O ²⁻	529.70	0.3581	0.0
Zn ²⁺ -Zn ²⁺	0.0	0.0	0.0

simulation of phase transformations in nanorods with high surface-to-volume ratios.

In the classical approximation ($\hbar\omega \ll kT$), Eq. (1) can be rewritten as

$$F \approx \Phi + kT \sum_{j=1}^N \sum_{\alpha=1}^3 \ln \left(\frac{\hbar\omega_{j\alpha}}{kT} \right), \quad (3)$$

where the frequencies of oscillation for the atoms are the $3N$ eigenvalues which can be obtained from the diagonalization of the dynamical matrix \mathbf{D} ^{17,18,21} in the form of

$$D_{ij}^{\alpha\beta} = \frac{1}{\sqrt{m_i m_j}} \left(-\frac{\partial^2 \Phi}{\partial r_{i\alpha} \partial r_{j\beta}} \right). \quad (4)$$

In the above expression, m_i is the mass of atom i and $r_{i\alpha}$ is the α th coordinate of atom i .

When N is large, the diagonalization is extremely difficult. To strike a balance between accuracy and efficiency like those in Refs. 16–18, 21, and 22 we adopt the local harmonic approximation by rewriting Eq. (3) as

$$F \approx \Phi + 3kT \sum_{i=1}^N \ln \frac{\hbar |D_i|^{1/6}}{kT}, \quad (5)$$

where D_i is the determinant of the local dynamical matrix of atom i . The statistical equilibrium configurations under the conditions of macroscopic quasistatic deformation and associated thermomechanical quantities can be obtained by minimizing this Helmholtz free energy. Mathematically, this entails setting the derivatives of F with respect to $r_{i\alpha}$ at fixed temperature and boundary loading to zero, i.e.,

$$\frac{\partial \Phi}{\partial r_{i\alpha}} + \frac{1}{2} \frac{kT}{|D_i|} \frac{\partial |D_i|}{\partial r_{i\alpha}} = 0, \quad i = 1, \dots, N, \quad \alpha = 1, 2, 3. \quad (6)$$

In the MST algorithm used here, the deformation is strain controlled and the analysis is carried out at fixed levels of boundary displacement. The progression of deformation is achieved through displacement increments which correspond to a nominal strain increment of 0.25% during loading (−0.25% during unloading). This procedure is repeated until failure occurs for loading or the rod is fully unloaded for unloading.

B. Microstructure analysis

The microstructures of the ZnO nanorods are analyzed using the radial distribution function (RDF),

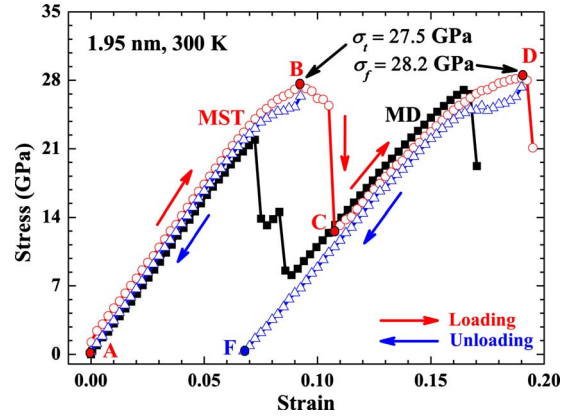


FIG. 2. (Color online) Stress-strain curves for the 1.95 nm nanorod. The black curve is obtained from MD simulation and the red line is from MST calculation, the blue curves are for unloading obtained using MST. The coincidence of the loading and unloading paths indicates elasticity without structural change.

$$g(r) = \frac{n(r, r + dr)}{V_S} \frac{N}{V}, \quad (7)$$

where n is the number of atoms in a spherical shell with thickness dr , r is the distance from the atom at origin, V_S is the volume of the spherical shell, and N and V are the total number of atoms and total volume of the sample, respectively. Peaks of RDF represent the ratio of the radial density of atoms at distance r to the mean density of atoms. The dominant lattice parameters (a , b , and c) of different structures can be identified from the positions of their corresponding peaks. The widths of the peaks are related to the deviations of atomic positions from the dominant lattice distances.

III. RESULTS AND DISCUSSIONS

A. Phase transformation from WZ to tetragonal structure

As illustrated in Fig. 2, the results of MST simulation show three-stage stress-strain relations which are similar to that obtained from the previous MD simulations.⁷ The particular rod size analyzed in the figure is 1.95 nm. The first stage (A→B) corresponds to the elastic stretching of the WZ-structured rod up to a strain of $\epsilon_t = 9.25\%$ with a characteristic stress $\sigma_t = 27.5$ GPa. This is the critical stress required for the nucleation of a new tetragonal phase in the rod. This phase is previously referred to as a body-centered-tetragonal structure with four-atom rings (BCT-4) and belongs to the P42/mmm space group.^{7,8} Further loading leads to a precipitous drop in stress (B→C), indicating the progression of the structural transformation from WZ to the tetragonal structure. It should be pointed out that, strictly speaking, this new crystalline structure is not body-centered-tetragonal. Rather, the space group P42/mmm is fully tetragonal, with primitive cell parameters $a = b$ and $\alpha = \beta = \gamma = 90^\circ$. The parameters for the Wyckoff positions of zinc and oxygen atoms are identical. The lattice would be body-centered-tetragonal (space group I4/mmm) if all atoms are of the same species. A description of how the transformation occurs

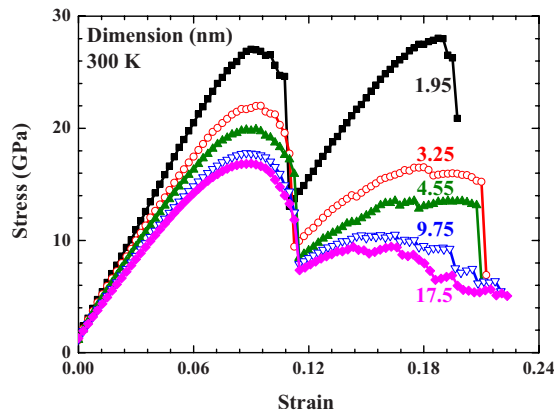


FIG. 3. (Color online) Stress-strain curves from MST simulations for different cross-sectional diameters between 1.95 and 17.5 nm.

has been given in Ref. 7. Similar tetragonal structures have been reported for BeO,²⁶ carbon,²⁷ and lithium aluminum oxide.²⁸

B. Size dependence

Since rod sizes smaller than 4.55 nm have been analyzed through MD simulations in previous works,^{7,8} the focus here is on sizes larger than 4.55 nm which cannot be easily analyzed by MD due to prohibitively large central processing unit (CPU) requirements. Figure 3 shows the stress-strain curves for five sizes between 1.95 and 17.5 nm from MST simulations. A significant dependence of behavior on size is seen. The critical stress required to initiate the transformation (σ_t) decreases by 39.3% from 27.5 to 16.7 GPa as the size increases from 1.95 to 17.5 nm. The failure stress (σ_f) shows an even stronger dependence on size, decreasing 66.5% from 28.2 to 9.44 GPa over the same size range [see Fig. 4(a)]. The Young's modulus of WZ-structured rods (E_W) decreases 30% from 310 to 217 GPa and the Young's modulus of the tetragonal-structured (TS) rods (E_T) decreases 70.6% from 250 to 73.5 GPa as the lateral dimension increases from 1.95 to 17.5 nm [see Fig. 4(b)].

This size dependence of Young's modulus in ZnO nanorods with WZ structure revealed by MST simulations is compared with that observed in experiments.¹⁹ Since the smallest diameter of nanorods tested experimentally is limited to about 17 nm, the MST results here just provide the Young's modulus for nanorods below this size. The Young's modulus from both MST results and experimental tests¹⁹ as a function of nanorod diameter is plotted in Fig. 5. For the largest sample in the MST simulations (which is the smallest size tested in experiments), the calculated Young's modulus is 217 GPa, in good agreement with the experimentally measured value of 221 GPa. A core-shell model was proposed¹⁹ to explain this size dependence by considering the surface effects. However this model does not work for the MST results, because the assumption of uniform modulus for the structure in the core and shell regions in the model is not suitable for nanorods with lateral diameter less than 20 nm.²⁹

The stress-strain curves after the phase transformation show an even stronger size dependence (see Fig. 3). Both the failure stress (σ_f) and the slopes of the curves decrease sig-

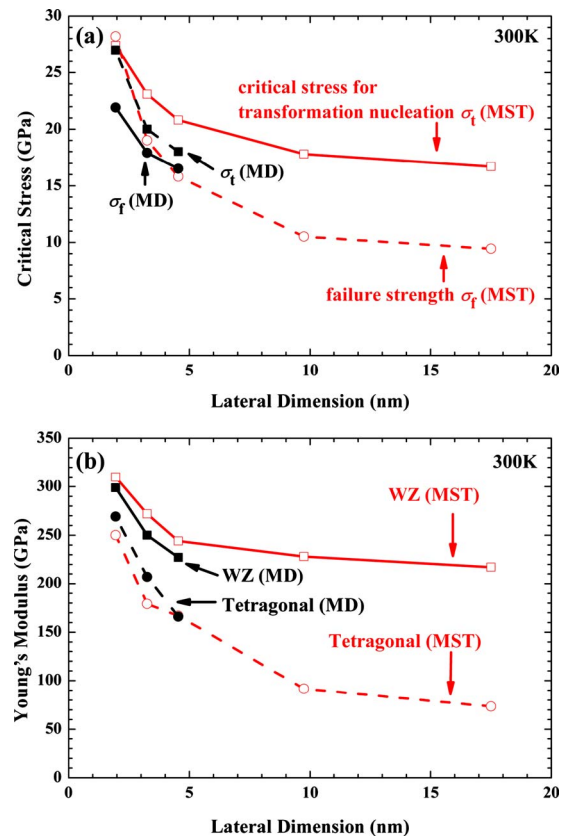


FIG. 4. (Color online) (a) Critical stresses for nucleation of phase transformation and failure as functions of wire size. (b) Young's modulus as a function of wire size.

nificantly as the size increases. This is primarily attributed to the fact that the tetragonal structure after the transform is polycrystalline in nature and grains of different sizes and orientations exist, as seen on the cross sections with different lateral sizes in Fig. 6. The orientations of grains with the transformed tetragonal structure are denoted by the [001] direction (normal to the four-atom rings) of the tetragonal structure.^{7,8} A ring is regarded as belonging to a grain only if it is at the geometric center of eight other first neighbor

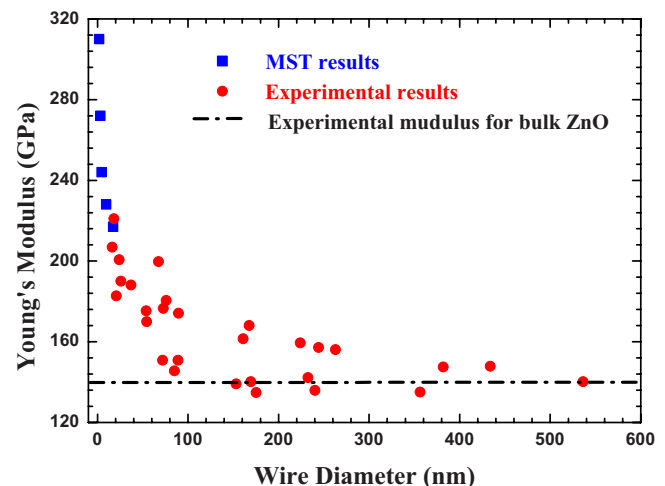


FIG. 5. (Color online) Variation of Young's modulus with wire diameter (Ref. 19) (the dash-dotted line denotes the experimentally reported bulk value of about 140 GPa).

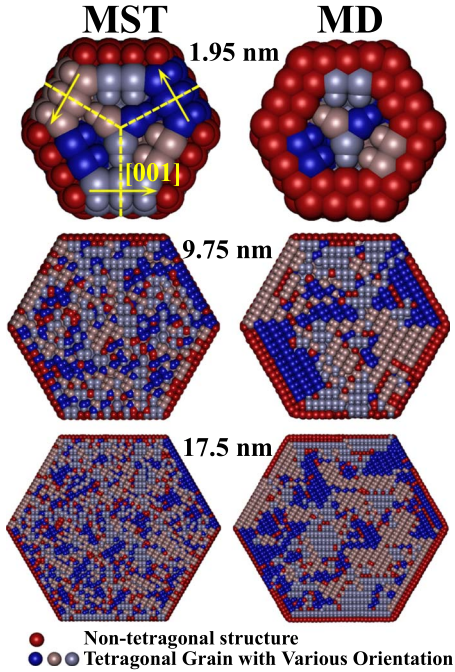


FIG. 6. (Color online) Cross-sectional view of rod structures immediately after the phase transformation. Atoms in red are either surface atoms or interior atoms not belonging to the tetragonal structure. Other colors denote tetragonal grains with different [001] orientations.

rings. At the smallest size (1.95 nm), the whole rod transforms from the WZ to the tetragonal phase immediately after the transition strain (ε_t) and further loading reveals only the behavior of the pure tetragonal structure. At larger rod sizes, the transformation occurs gradually in different regions. At any subsequent strain (e.g., 11.5% of the 17.5 nm rod in Fig. 6), there are both WZ- and tetragonal-structured regions in rods larger than 1.95 nm, with the tetragonal-structured grains showing different sizes and orientations. Continued deformation of the rods occurs through the nucleation of new tetragonal regions as well the reorientation, growth, and coalescence of existing tetragonal-structured grains.

C. Comparison of the results from MST and MD

The lattice parameters for the two phases obtained from MST, MD, and DFT calculations are listed in Table III. The results from MST are consistent with those from MD and DFT,⁸ with only minor errors of less than 3%.

Overall, the MST and MD simulations yielded results with similar features, including the phase transformation, average properties (such as Young's modulus and unloading

TABLE IV. A comparison of results from MST and MD.

Similarities	(1) Three-stage stress-strain relation and elastic unloading
	(2) Transformation from WZ to tetragonal structure under tensile loading
	(3) Consistent lattice parameters for WZ and tetragonal structures (errors <1% between MST and DFT and <3% between MST and MD)
	(4) Consistent Young's modulus values (see Fig. 4)
	(5) Consistent size effect trend predictions: as size increases, critical stresses for phase transformation, tensile strength and Young's modulus decrease
Differences	(1) Critical stress for phase transformation in MST is over 25% greater than that in MD
	(2) Tensile strength in MST shows various differences compared to that in MD (see Fig. 4)
	(3) The efficiency of MST is almost 60 times that of MD

behavior), and size effect trend (as shown in Fig. 4 and Table IV). This consistency of tendency lends credence to the MST method and results. However, there are some differences in the MST and MD results for critical quantities such as the stress for phase transformation σ_t and strength σ_f . For example, the onset of both σ_t and σ_f obtained from MST lags behind that predicted by MD (Fig. 2). A look at the basics of the two methods helps understand the difference. In MD, the thermal motions of atoms play a key role in overcoming the energy barriers to phase transformations. After each loading or unloading increment, the nanorod must be relaxed for a considerable period to allow a statistical equilibrium state to be reached and time-averaged values for quantities such as stress, energy, and temperature to be extracted. In MST, on the other hand, the preferred configuration of the atomistic system is obtained via the minimization of the Helmholtz free energy. The values extracted are spatially and temporarily averaged macroscopic equilibrium values. Either stable or metastable states can be reached and the contributions of thermal motions of atoms are accounted for only through a phenomenological characterization of their thermal energies in aggregate as oscillators. Therefore, MST may yield locally metastable states as well as global stable states, whereas MD is more likely to identify lowest energy, globally stable equilibrium states through explicit account of all possible paths and modes of atomic motions. Because of this reason, MST simulations tend to yield an upper bound to the critical stress of phase transformation, as seen in Fig. 2.

To ascertain the stability of the atomic configuration obtained by MST after the phase transformation, MD calcula-

TABLE III. Lattice parameters of WZ and tetragonal structures.

		a (Å)	b (Å)	c (Å)	b/a	c/a
WZ, point A in Fig. 2	MST	3.26	5.61	5.18	1.72	1.59
	MD	3.25	5.65	5.20	1.73	1.60
	DFT	3.20	5.55	5.13	1.73	1.60
Tetragonal structure, point F in Fig. 2	MST	3.18	5.52	5.53	1.74	1.74
	MD	3.26	5.66	5.62	1.74	1.69
	DFT	3.17	5.48	5.48	1.73	1.73

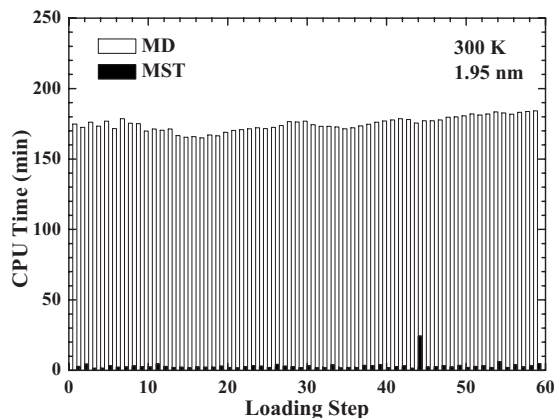


FIG. 7. A comparison of CPU time consumption by MD and MST. At the 44th load step, phase transformation occurs, causing MST to require more computations to find the minimum free energy state.

tions are carried out for the 9.75 and 17.5 nm rods near the critical point for transformation initiation. Specifically, configurations of these rods at a strain of 6.5% are first obtained from MST calculations and relaxed. At this strain level, the rods are still fully WZ-structured. Subsequently, MD loading up to a strain of 9.0% is carried out to achieve full transformation in the rods. Figure 6 shows the configurations upon transformation completion obtained from MST and MD. The 3.25 and 4.55 nm rods are not shown due to space limitation. In general, fewer surface atoms are involved in the WZ-to-tetragonal structure transformation in the MD results than in the MST results. This can be seen from rods of all sizes shown. Also, the MD calculations yielded larger tetragonal grains than MST. This can be explained by the fact that MD better captures the more stable/lower energy structures of materials than MST. In contrast, MST leads more to metastable structures along the paths to the more stable states with the lowest free energies. Overall, however, the MD and MST calculations show consistent results in that both demonstrate the same WZ-tetragonal structure transformation and lead to polycrystalline structures with WZ and tetragonal grains with different orientations. Furthermore, both show the same trend of the grains becoming more evenly distributed as the rod size increases.

The computational efficiencies of MST and MD are also compared. Figure 7 shows the CPU time requirements of MST and MD for calculations for a 1.95 nm rod using 32 processors on an Itanium[®] 2 based parallel cluster. Obviously, MST is approximately 60 times faster than MD for the same problem, suggesting its advantages for large problems under quasistatic loading conditions at finite temperatures. Furthermore, it is conceivable that a combination of MST and cluster statistical thermodynamics (CST)^{16,18} may allow a range of problems with sizes up to microns to be analyzed in the near future.

IV. CONCLUSIONS

The MST method, a numerical technique for macroscopic quasistatic conditions at finite temperatures, has been used to analyze the deformation of ZnO nanowires with the [0001]-growth orientation under tensile loading. The wires

analyzed have lateral dimensions ranging from 1.95 to 17.5 nm. The size dependence of Young's modulus before the WZ-to-tetragonal structure transformation is in general good agreement with that observed in experiments. The distributions of tetragonal-structured grains in larger (from 3.25 to 17.5 nm) transformed nanorods lead to more gradual increases in stress with strain as the size increases. The mechanism leading to this involves the nucleation, growth, deformation, and movement of tetragonal-structured grains and interactions between grains and defects. A comparison of the MST and MD methods shows that the MST method yields results qualitatively and quantitatively consistent with the results from MD simulations. In particular, the MST framework is shown to be capable of identifying the WZ-to-tetragonal phase transformation originally predicted by MD and DFT calculations. The numerical differences between results of MST and MD indicate that the phenomenological nature of MST in quantifying the thermal motions of atoms may affect and limit its identification of all possible routes to equilibrium states, especially in regard to phase transformations and failure. One advantage of MST is that it can be up to 60 times faster than MD in calculations, therefore, potentially allowing material systems with larger size scales to be analyzed.

ACKNOWLEDGMENTS

Support from the National Natural Science Foundation of China (NSFC) (Grant Nos. 10772012, 10732090, 10772181, and 10721202), the Chinese Academy of Sciences (CAS) Innovation Program (Grant No. KJCX2-YW-M04), the National Basic Research Program of China (Grant No. 2007CB814803), the U.S. NSF (Grant No. CMS9984298), and KOSEF (Grant No. R31-2008-000-10083-0) is gratefully acknowledged. Computations are performed on computer clusters at the State Key Laboratory for Scientific and Engineering Computing of the CAS, the Supercomputing Center of the CAS (CNIC), and the Dynamic Properties Research Laboratory at Georgia Tech.

¹A. Wei, X. W. Sun, C. X. Xu, Z. L. Dong, Y. Yang, S. T. Tan, and W. Huang, *Nanotechnology* **17**, 1740 (2006).

²A. Ashrafi and C. Jagadish, *J. Appl. Phys.* **102**, 071101 (2007).

³S. Limpijumng and S. Jungthawan, *Phys. Rev. B* **70**, 054104 (2004).

⁴C. L. Freeman, F. Claeysens, N. L. Allan, and J. H. Harding, *Phys. Rev. Lett.* **96**, 066102 (2006).

⁵A. J. Kulkarni, M. Zhou, K. Sarasamak, and S. Limpijumng, *Phys. Rev. Lett.* **97**, 105502 (2006).

⁶A. J. Kulkarni, K. Sarasamak, J. Wang, F. J. Ke, S. Limpijumng, and M. Zhou, *Mech. Res. Commun.* **35**, 73 (2008).

⁷J. Wang, A. J. Kulkarni, F. J. Ke, Y. L. Bai, and M. Zhou, *Comput. Methods Appl. Mech. Eng.* **197**, 3182 (2008).

⁸J. Wang, A. J. Kulkarni, K. Sarasamak, S. Limpijumng, F. J. Ke, and M. Zhou, *Phys. Rev. B* **76**, 172103 (2007).

⁹Z. L. Wang and J. Song, *Science* **312**, 242 (2006).

¹⁰E. B. Tadmor, M. Ortiz, and R. Phillips, *Philos. Mag. A* **73**, 1529 (1996).

¹¹L. M. Dupuy, E. B. Tadmor, R. E. Miller, and R. Phillips, *Phys. Rev. Lett.* **95**, 060202 (2005).

¹²F. Abraham, J. Broughton, N. Bernstein, and E. Kaxiras, *Comput. Phys.* **12**, 538 (1998).

¹³L. Shilkrot, W. Curtin, and R. Miller, *J. Mech. Phys. Solids* **50**, 2085 (2002).

¹⁴W. Curtin and R. Miller, *Model. Simul. Mater. Sci. Eng.* **11**, R33 (2003).

¹⁵R. Rudd and J. Broughton, *Phys. Rev. B* **72**, 144104 (2005).

¹⁶M. Hu, H. Wang, M. Xia, F. Ke, and Y. Bai, *Cluster Statistical Thermo-*

- dynamics (CST): To Efficiently Calculate Quasi-Static Deformation at Finite Temperature Based on Molecular Potentials* (Springer, Beijing, 2005), p. 163–170.
- ¹⁷H. Y. Wang, M. Hu, M. F. Xia, F. J. Ke, and Y. L. Bai, “*Molecular Statistical Thermodynamics (MST): A Fast Converging Molecular Simulation for Quasi-Static Deformation at Finite Temperature*, The 2nd International Conference on Scientific Computing and Partial Differential Equations & The First East Asia SIAM Symposium, Hong Kong, 2005).
- ¹⁸H. Wang, M. Hu, M. Xia, F. Ke, and Y. Bai, *Int. J. Solids Struct.* **45**, 3918 (2008).
- ¹⁹C. Q. Chen, Y. Shi, Y. S. Zhang, J. Zhu, and Y. J. Yan, *Phys. Rev. Lett.* **96**, 075505 (2006).
- ²⁰D. A. McQuarrie, *Statistical Mechanics* (Harper & Row, New York, 1976).
- ²¹R. LeSar, R. Najafabadi, and D. J. Srolovitz, *Phys. Rev. Lett.* **63**, 624 (1989).
- ²²L. Zhao, R. Najafabadi, and D. J. Srolovitz, *Modell. Simul. Mater. Sci. Eng.* **1**, 539 (1993).
- ²³D. J. Binks and R. W. Grimes, *J. Am. Ceram. Soc.* **76**, 2370 (1993).
- ²⁴D. J. Binks, Ph.D. thesis, University of Surrey, 1994.
- ²⁵A. J. Kulkarni, M. Zhou, and F. J. Ke, *Nanotechnology* **16**, 2749 (2005).
- ²⁶D. K. Smith, C. F. Cline, and S. B. Austerman, *Acta Crystallogr.* **18**, 393 (1965).
- ²⁷P. A. Schultz, K. Leung, and E. B. Stechel, *Phys. Rev. B* **59**, 733 (1999).
- ²⁸M. Marezio and J. P. Remeika, *J. Chem. Phys.* **44**, 3348 (1966).
- ²⁹R. Agrawal, B. Peng, E. Gdoutos, and H. Espinosa, *Nano Lett.* **8**, 3668 (2008).